Respiratory tract explant infection dynamics of influenza A virus in California sea lions, northern elephant seals, and rhesus macaques and severe acute respiratory syndrome virus-2 in rhesus macaques

Hongwei Liu[1] , Magdalena Plancarte[1] , Erin. E. Ball[1] , Christopher M. Weiss[1], Omar Gonzales-Viera[1], Karen Holcomb[1], Zhong-Min Ma[2], A. Mark Allen[2], J. Rachel Reader[2], Pádraig J. Duignan[3], Barbie Halaska[3], Zenab Khan[4], Divya Kriti[4], Jayeeta Dutta[4], Harm van Bakel[4], Kenneth Jackson[1], Patricia A. Pesavento[1], Walter M. Boyce[1], Lark L. Coffey[1#]

[1]University of California, Davis, School of Veterinary Medicine, Department of Pathology, Microbiology and Immunology

[2]University of California, Davis, California National Primate Research Center

[3]The Marine Mammal Center, 2000 Bunker Road, Sausalito, California

[4]Icahn School of Medicine at Mount Sinai, New York, New York

[#]Corresponding author

lcoffey@ucdavis.edu

ORCID numbers:

Lark L. Coffey : 0000-0002-0718-5146

Erin E. Ball: 0000-0002-8464-6612

Karen M. Holcomb: 0000-0002-9403-3756

Hongwei Liu: 0000-0002-8342-2545

Abstract

To understand susceptibility of California sea lions and Northern elephant seals to influenza A virus (IAV), we developed an *ex vivo* respiratory explant model and used it to compare infection kinetics for multiple IAV subtypes. We used a similar approach with explants from rhesus macaques to establish the system and to compare infection kinetics with marine mammals. Trachea, bronchi, and lungs from 11 California sea lions, 2 Northern elephant seals and 10 rhesus macaques were inoculated within 24 hours post-mortem with 6 strains representing 4 IAV subtypes. Explants from all 3 species showed similar IAV infection kinetics with peak viral titers 48-72 hours post-inoculation (hpi) that increased by 2-4 $\log_{10}$ PFU/explant relative to the inoculum. Immunohistochemistry localized IAV infection to apical epithelial cells. These results demonstrate that respiratory tissue explants from marine mammals support IAV infection. In the absence of the ability to perform experimental infections of marine mammals, this *ex vivo* culture of respiratory tissues mirrors the *in vivo* environment and serves as a tool to study IAV susceptibility, host-range, and tissue tropism. We adapted the explant approach and used it to inoculate tissues from 2 rhesus macaques with severe acute respiratory syndrome virus 2 (SARS-CoV-2). SARS-CoV-2 titers increased by 2-4 $\log_{10}$ PFU/explant relative to the inoculum and peaked 48 or 72 hpi in trachea, bronchi, and kidney of both macaques and in the lung of 1 animal. These results demonstrate that this *ex vivo* model can define infection dynamics for 2 respiratory viruses of significant public health importance.

Importance

Although influenza A virus can infect marine mammals, a dearth of marine mammal cell lines and ethical and logistical challenges prohibiting experimental infections of living marine mammals means that little is known about IAV infection kinetics in these species. We circumvented these limitations by adapting a respiratory tract explant model first to establish the approach with rhesus macaques and then for use with marine mammals. We observed that multiple strains representing 4 IAV subtypes infected trachea, bronchi, and lungs of macaques and marine mammals with variable peak titers and kinetics. We adapted the approach for SARS-CoV-2 and observed that the infection kinetics in inoculated rhesus macaque explants parallel observations from *ex vivo* human lungs. This *ex vivo* model can define infection dynamics for 2 respiratory viruses of significant public health importance and use of explants from animals euthanized for other reasons reduces use of animals in research.

Introduction

Influenza A viruses (IAV) are important etiologies of respiratory disease in humans and especially affect the elderly, infants, and people with immunodeficiencies and chronic respiratory disease. Dwarfed in 2020 by SARS-CoV-2, IAV are a significant cause of morbidity annually, producing about 500,000 deaths worldwide each year (1). IAV possess a wide host range that includes birds, horses, pigs, and humans (2, 3). Marine mammals can also be infected, sometimes with strains from human pandemics (4, 5). The viral genetic and host factors that affect cross-species transmission by IAV, especially from birds to mammals including humans, have been extensively studied (5–9). However, mechanisms of zoonotic IAV transmission from avian or human to other mammalian species, including marine mammals, are less well understood (6).

IAV was first identified in North American marine mammals in 1979, when an H7N7 epizootic killed 500 harbor seals and caused hemorrhagic pneumonia in others (10–12). Since then, IAV infection and sometimes disease has been identified in several marine mammal species, including mass mortalities in harbor seals near Cape Cod, Massachusetts, USA, attributed to H7N7, H4N5, or H4N6, and detection of antibody to multiple H and N subtypes in several seal species (13–20). On the West Coast, surveillance from 2009 to 2015 (4, 21, 22), and from 2016 to present (unpublished) in multiple marine mammal species from California shows variable IAV exposure. Seroprevalence in sea otters and Northern elephant seals is higher than in sympatric harbor seals and California sea lions, and sea otters are exposed to avian- and human-origin IAV, including pandemic H1N1 (4, 21). Despite frequent antibody detection, isolation of IAV from marine mammals has been limited. In California, only pandemic H1N1 has been isolated from 2 Northern elephant seals in 2010 (4). Together, these surveillance data suggest that marine mammals sometimes become infected with some of the same IAV subtypes that cause human epidemics. However, in the absence of *in vivo* study capabilities in marine mammals, infection dynamics and subtype-specific susceptibility remain unknown.

Given that the respiratory tract is the initial site of IAV infection, defining infection dynamics and cellular tropism in respiratory tissues is important for assessing species susceptibility. However, *in vivo* systems for studying susceptibility of marine mammals to IAV are not available. As an alternative, *ex vivo* explants from respiratory tract tissues can mimic the physiological microenvironment of a respiratory tract. *Ex vivo* systems in human and animals (excluding

marine mammals) have been successfully developed and used to study host innate responses, infection dynamics, viral genetic determinants of infection, antiviral drug treatments, and pathogenesis of human and animal IAV (23–28). The goal of this study, therefore, was to expand these existing models for use in marine mammals to study susceptibility and infection dynamics of IAV. Since marine mammal tissues are only opportunistically available from animals at The California Marine Mammal Center in Sausalito, CA, USA, we first established the *ex vivo* explant system using rhesus macaques that are more regularly available from the California National Primate Research Center, Davis, CA, USA. Furthermore, rhesus macaques represent a valuable model for understanding IAV infection dynamics in the human respiratory tract due to similar structure, physiology, and mucosal immunity. When SARS-CoV-2 that causes COVID-19 emerged globally in 2020, we also expanded the explant system to characterize SARS-CoV-2 infection dynamics in rhesus macaques, who also exhibit clinical COVID-19-like disease after experimental inoculation (29–31).

We used trachea, bronchi, and lung explants from rhesus macaques to compare the susceptibility, infection kinetics, and tissue tropism of 6 strains of IAV from 4 subtypes to validate the utility of this system. After establishing the explant approach with IAV in rhesus macaques, we used it to study IAV infection dynamics and tropism in California sea lions and Northern elephant seals and to validate its use for SARS-CoV-2 in rhesus macaques.

Material and Methods

Ethics Statement

This project was conducted with approval from the United States National Marine Fisheries Service Marine Mammal permit # 18786-04. The University of California, Davis is accredited by the Association for Assessment and Accreditation Laboratory Animal Care International (AAALAC). Animal care was performed in compliance with the 2011 Guide for the Care and Use of Laboratory Animals provided by the Institute for Laboratory Animal Research. Rhesus macaque studies were approved by the University of California, Davis IACUC under protocol #19760.

Explant sources, collection and processing

Respiratory tract tissues including trachea, bronchi, and lungs were used for explant studies **(Table 2**). Tissues were obtained from Indian origin rhesus macaques (*Macaca mulatta*), euthanized due to

medical conditions, who were born and raised at the California National Primate Research Center, University of California, Davis, CA. The respiratory tract tissues from California sea lions (CSL, *Zalophus californianus*) and Northern elephant seals (NES, *Mirounga angustirostris*) were obtained from patients euthanized due to medical conditions, at The Marine Mammal Center, Sausalito, CA. Tissues from all three species were stored for up to 24 hours in Roswell Park Memorial Institute-1640 (RPMI) medium (Gibco) at 4°C. Prior to preparation for infection studies, tissues were separated and washed 4-6 times in 50 ml conical tubes containing 30 ml of RPMI medium. The final wash was performed in RPMI-growth-medium (RPMI medium supplemented with 100 U/ml each of penicillin and 100 ug/ml streptomycin (Gibco) and 1x antibiotic-antimycotic (Gibco)) for 2-5 min each at room temperature in a biosafety cabinet.

Preparation of tracheal and bronchi explants

A simplified *ex vivo* culture procedure was derived from the methods described by Nunes *et al*. (Nunes et al, 2010). After washing in RPMI medium, the surrounding connective tissue exterior to the tracheal and bronchi cartilage was removed. Trachea were cut into O-rings horizontally where each slice contained about 0.5 cm cartilage. Each O-ring consisted of the respiratory mucosa, epithelial cell layer, and underlying cartilage. O-rings were further cut into small pieces of approximately 0.5 cm x 0.5 cm. Bronchi were cut similarly. Explants were implanted singly into agarose plugs (RPMI-growth-medium containing 0.5 % agarose) in 24-well plates with the mucosal surface facing up. Explants were maintained in a humidified 37°C incubator with 5% CO_2 for up to 7 days.

Preparation of lung, liver, and kidney explants

Lung tissues were used to investigate IAV tissue specificity. Processing was the same as for upper respiratory tissues, lung tissues were cut into pieces of approximately 0.5 cm^3 after washing. Each piece was implanted onto agarose plugs and incubated using the same conditions as for trachea and bronchi. The liver and kidney of two rhesus macaques were used as non-target tissue controls where IAV infection was not expected.

Cell culture

For IAV culture, Madin-Darby Canine Kidney (MDCK) cells (ATCC #CCL-34) were maintained at 37°C and 5% CO2 in MDCK-growth-medium (Iscove's Modified Dulbecco's Medium (IMDM), supplemented with 5% FBS, 0.1% sodium bicarbonate, penicillin and streptomycin). For SARS-

CoV-2 culture, Vero (ATCC #CCL-81) and Vero E6 (ATCC# CRL-1586) cells were maintained in Vero-growth-medium (Dulbecco's modified Eagle's medium (DMEM; Gibco), supplemented with 5% FBS, 0.1% sodium bicarbonate (Gibco), 10 mM of HEPES (4-(2-hydroxyethyl)-1-piperazineethanesulfonic acid (Gibco), and 1X antibiotic/antimycotic (Gibco).

Influenza A virus propagation and titration

We used IAV strains of avian and marine mammal origin for explant studies (**Table 1**). The harbor seal H3N8 (HS/H3N8) IAV strain was obtained from Dr. Hon Ip, (National Wildlife Health Center, Madison Wisconsin). The other strains were isolated at UC Davis by our team. Avian allantoic fluid virus stocks of 6 strains were amplified in Madin-Darby canine kidney (MDCK) cells to obtain sufficient titers and volumes for use as inocula. Viral titers of the 6 inocula were determined by plaque assay using MDCK cells. Briefly, MDCK cells were grown in 6-well plates to 80-90% confluence in MDCK growth medium. Viral stocks were serially ten-fold diluted in viral-growth-medium (Minimum Essential Medium (MEM), supplemented with 0.5% BSA, 0.1% sodium bicarbonate, 10 mM Hepes, penicillin and streptomycin). The MDCK cells were washed 3 times with Dulbecco's phosphate buffered saline (DPBS) prior to inoculation with 200 ul of diluted virus samples. After 1 hour incubation at 37°C with 5% CO_2, 3 ml viral-growth-medium containing 1 ug/ml N-p-tosyl-L-phenylalaninechloromethyl ketone-treated (TPCK) and 0.5% agarose was added to each well. After a 48 hour incubation at 37°C with 5% CO_2, the MDCK cells were fixed with 4% formaldehyde and stained with 0.05% crystal violet.

SARS-CoV-2 propagation and titration

A SARS-CoV-2 strain (human/USA/CA-CZB-59X001/2020 (MT394529) that was provided by Chris Miller at the California National Primate Research Center was propagated in Vero E6 cells to produce working stock. Vero E6 cells were inoculated at a multiplicity of infection (MOI) of 0.01 and incubated for 48 hours. At 48 hpi, the culture supernatant was cleared by centrifugation and stored in aliquots at −80°C. Stock titers were determined by plaque assay using Vero cells as described previously for chikungunya virus (32).

Titration quantification

Plaques were counted against a white background and the titer in plaque forming units (PFU) was determined by counting wells with individual plaques. Two to 3 dilutions of each explant were tested once. Viral titers were recorded as the reciprocal of the highest dilution where plaques are noted and

represented as PFU per ml for liquid samples or PFU per explant for tissues. The limit of detection (LOD) of the assay for IAV was 50 PFU/ml or explant and 80 PFU/ml or explant for SARS-CoV-2.

In vitro infection kinetics of IAV and SARS-CoV-2

Infection kinetics for the 6 IAV strains and 1 SARS-CoV-2 strain were assessed in MDCK and Vero E6 cells, respectively. Both cell types were grown at 37°C with 5% CO_2 to 6 x 10^5 cells/well in 24-well plates and inoculated in triplicate with 6 x 10^3 PFU virus of IAV, representing a multiplicity of infection (MOI) of 0.01, or 6 x 10^3, 6 x 10^4, or 6 x 10^5 PFU of SARS-CoV-2, representing MOIs of 0.01, 0.1 or 1, respectively. After 1 hour incubation, each well was washed with 1 ml of DPBS 3 times to remove unbound virus. Next, viral growth medium supplemented with 1 ug/ml TPCK trypsin for IAV or Vero-growth medium for SARS-CoV-2 was added to each well. The supernatant was sampled at 1, 24, 48, and 72 hours post-inoculation and then diluted and frozen at -80°C in virus growth medium. Viral titers were assessed by plaque assay.

Ex vivo IAV or SARS-CoV-2 infection kinetics

To evaluate IAV or SARS-Cov-2 infection kinetics *ex vivo*, trachea, bronchi, and lung explants were inoculated in triplicate (when sufficient tissue was available) with 1 x 10^4 PFU of one of each of the 6 IAV strains or 1 SARS-CoV-2 strain in 10 ul viral growth medium onto the epithelial surface of each section for rhesus macaques. The inoculum volume for marine mammals was adjusted to 20 ul at a dose of 2 x 10^4 PFU of each IAV strain. Viral growth medium was used in the mock-infected control explants. Inoculated explants were sampled at 1 hour post infection (hpi) and every 24 hours up to 72 hpi (or as indicated in graphs) for viral quantification and histology. For viral quantification, each infected explant (for both IAV and SARS-CoV-2) was directly immersed in 0.5 ml RPMI-growth-medium in a 2 ml centrifuge tube with a 5 mm glass bead and homogenized in a Mixer Mill MM300 (Retsch, Leeds, UK) at 30 hertz for 4 minutes at 22°C followed by centrifugation at 16,000 g for 4 minutes and storage at -80°C. Titers of the released progeny virus from explants were determined by plaque assay. Titers are reported as the geometric mean of triplicate explants at each time point.

Stability assays

To determine whether IAV detected after inoculation was due to productive virus infection in respiratory tissues, we performed viral stability assays in the absence of tissue sections. Medium containing 1 X 10^4 PFU/ml of each of the 6 IAV strains was added to 24-well tissue

culture plates and supernatant was collected at 0, 24 and 48 hpi for the determination of viral titers by plaque assay. As a second step, the stability assays were also performed using non-target tissues (liver and kidney) to confirm that the viral titers detected in respiratory tissues reflect productive infection in target cells. Liver and kidney explants were inoculated with 1 x 10^4 PFU of each of the 6 IAV strains or SARS-CoV-2 in 10 ul RPMI growth medium and assayed by the same methods used for respiratory tract tissues.

Influenza A Virus immunohistochemistry

Tracheal, bronchial, and lung explants from a subset of IAV-inoculated animals (M11, M13, SL08, and SL12) were fixed in 10% buffered formalin and embedded in paraffin. These animals were selected since they showed higher IAV titers than others. Antigen retrieval was performed on 5 um sections via incubation in AR10 (Biogenex) in a digital decloaking chamber (Biocare Medical) for 2 minutes at 125°C, followed by cooling to 90°C for 10 minutes, rinsing with water, and a final Tris-buffered saline with 0.05% Tween 20 rinse. Tissue sections were exposed to the primary rabbit anti-influenza A virus nucleoprotein antibody (LSBio), at a ratio of 1:250 with antibody diluent (Dako). Primary antibody was replaced by normal rabbit IgG (Invitrogen) to serve as a negative isotype control. Tris-buffered saline with 0.05% Tween 20 was used for all washes. Nonspecific binding sites were blocked with 5% bovine serum albumin (Jackson ImmunoResearch). Binding of the primary antibody was detected using Envision rabbit polymer with AEC as the chromogen (Dako). Each tissue section was evaluated independently by two pathologists. Sections from slides were visualized with a Zeiss Imager Z1 (Carl Zeiss). Digital images were captured and analyzed using Openlab software (Improvisation). Cells with nuclear immunoreactivity were considered positive. The positive cells in the epithelium of the trachea were manually counted. The area of the tracheal epithelium was measured. The number of positive cells was presented as cells per square millimeter of the epithelium.

SARS-CoV-2 Immunohistochemistry

Rhesus macaque lung explant: Ten µm of frozen tissue sections from lung of M31 were blocked for 1 hour in blocking buffer (2% BSA, 0.3% Triton X100 and 10% donkey serum in 1x PBS). Sections were incubated with rabbit anti-SARS nucleocapsid primary antibody (NB100-56576 Novus Biologicals) at 1:200 in PBS containing 10% donkey serum to serve as the antibody buffer at 4°C for 48 hours. Slides were washed 3 times with PBS and incubated with Alexa-488 conjugated donkey anti-rabbit secondary antibody (Invitrogen) at 1:200 in antibody buffer for 1 hour at room temperature. Slides were washed twice with PBS and mounted in Prolong Antifade mounting medium containing DAPI (Invitrogen). Samples were imaged on a Leica TCS SP8 STED 3X confocal microscope at the

Advanced Imaging Facility at University of California School of Veterinary Medicine. Images were analyzed and a Z stack was applied using ImageJ (Fiji).

Vero cells: Slides with SARS-CoV-2 inoculated Vero cells were incubated in blocking buffer (2% BSA, 0.3% Triton X100 and 10% donkey serum in 1x PBS) for 1 hour at room temperature. After blocking, slides were incubated in mouse anti-SARS-CoV-2 nucleocapsid antibody (Sino Biological, #40143-MM05) at a dilution of 1:200 in PBS containing 10% donkey serum to serve as the antibody buffer and incubated overnight at 4°C. Slides were washed 3 times with PBS and incubated with Alexa-488 conjugated donkey anti-mouse secondary antibody (Invitrogen) diluted 1:200 in antibody buffer for 1 hour at room temperature. Slides were washed twice with PBS and then mounted in DAPI Fluoromount-G (SouthernBiotech). Samples were imaged on a Leica TCS SP8 STED 3X confocal microscope at the Advanced Imaging Facility at University of California Davis School of Veterinary Medicine. Images were analyzed and Z stack was applied using ImageJ software (Fiji).

Influenza A virus genome sequencing

IAV RNA from inocula and homogenized explant samples harvested 48 to 96 hpi from selected animals for all 3 species were sequenced. Viral RNAs were extracted using the Magmax-96 AI/ND Viral RNA isolation kit (Applied Biosystems). Viral RNA extracts were used as a template for multi-segment RT-PCR reactions to generate all 8 genomic segments of IAV using procedures described previously (22, 33). Consensus sequences were generated at the Icahn School of Medicine at Mount Sinai, as described previously (34). Genome sequences from explant samples were compared to inocula.

Statistical analyses

Statistical analyses were conducted using GraphPad Prism software version 8. Two-way ANOVA with Dunnett's multiple comparisons tests were performed to compare the mean viral titers in explants at 24, 48 and 72 hpi to the mean titer 1 hpi as well as mean viral titers in MDCK cells for all 6 IAV strains at 24, 48 and 72 hpi. IAV titers in tissue explants were plotted at 0, 24, 48, and 72 hpi and mean area under the curve (AUC) was calculated for all titers above the assay limit of detection. Within individual tissues, mean AUC was compared by one-way ANOVA using Tukey's method for multiple comparisons between all IAV strains. Mean titers for IAV strains and tissues after inoculation of rhesus macaque and California sea lion explants were computed using R (35). Welch ANOVA with the Games-Howell post-hoc tests

were used to compare changes in mean log_{10} viral titers from 1 to 24, 48, and 72 hpi across IAV strains, tissues within species, and by IAV strain and tissue pairs between species.

Results

Influenza A virus strain selection

We first compared relative infection kinetics for the 6 IAV strains used here (**Table 1**). The strains used were selected since they represent common IAV subtypes, some of which infect humans. Strains were isolated from mallard ducks (m, N=4), an elephant seal (ES, N=1), or a harbor seal (HS, N=1), and they share similar passage histories in embryonated chicken eggs and MDCK cells. Our rationale for using IAV strains of avian origin in addition to strains from marine mammals is that waterbirds serve as primary reservoirs of IAV and they share shore environments with marine mammals. The ES H1N1 strain is a human pandemic IAV.

Influenza A virus strains exhibit differential growth in immortalized cells

Infection kinetics for each of the 6 IAV strains were assessed by inoculation into MDCK cells in triplicate at a MOI of 0.01 (**Figure 1**). The H3N8 strain isolated from a harbor seal (HS/H3N8), exhibited the slowest and lowest growth kinetics, peaking at 10^5 PFU/ml 48 hpi. The H1N1 strains showed the fastest and highest growth kinetics, peaking at $>10^7$ PFU/ml by 24 hpi. The viral infection kinetics of the other 3 strains tested, all of which were isolated from mallard ducks, were intermediate between HS/H3N8 and the 2 H1N1 strains. Titers for all strains were significantly higher than those for HS/H3N8 at one or more time points between 24-72 hpi (two way ANOVA). Given these data show that *in vitro* infection kinetics in an immortalized cell line are different for the 6 IAV strains used in this study, we sought to determine whether the growth patterns of these strains also differed in explant tissues from the 3 animal species.

Influenza A viruses infect rhesus macaque respiratory tract explants

We established the *ex vivo* explant infection system in respiratory tract tissues from rhesus macaques euthanized at the California National Primate Research Center due to non-respiratory medical conditions (**Figure 2A**). Although tissues were used within 6 h post-mortem, we microscopically visualized movement of glass beads by cilia placed atop tracheas from some macaques and verified viability at 24 and 48 hours, similar to Nunes *et al*. (23). To determine whether rhesus macaque explants support IAV infection and to define the kinetics of infection, we measured viral titers for 7 days (from 1 to 168 hpi) in explants from the first animal, an 11-year old female inoculated with HS/H3N8 (**Figure 2B**). We defined infection as detection of a kinetic increase in infectious IAV titer above the inoculum, 10^4 PFU. Titers increased over time in all 3 tissues and exceeded inocula from 48-168 hpi in trachea, from 24-

120 hpi in bronchi, and from 72-96 hpi in the lung. Maximal titers >10^5 PFU/tissue were detected in all 3 tissue types. Decreases in titers over time were likely concomitant with death of target cells in explants. By contrast, when 10^4 PFU of IAV strains were inoculated into medium in the absence of explants (**Figure 2C**) or into non-IAV target kidney (**Figure 2D**) or liver (**Figure 2E**) from a 3.5 year old macaque, no IAV was detected above the limit of detection (50 PFU/explant) at 24 or 48 hpi. Together these results demonstrate that rhesus macaque respiratory tract explants support productive infection by IAV.

Influenza A virus exhibits strain-specific infection patterns in ex vivo respiratory tract tissues

Rhesus macaques: To determine whether rhesus macaques share similar susceptibilities to different IAV subtypes, we inoculated respiratory tract explants from 10 rhesus macaques (**Table 2**) with 6 virus strains. Five of the macaques were females and five were males, they ranged from 1 to 16 years of age, and most were euthanized due to injuries sustained due to non-respiratory conditions including trauma or chronic diarrhea. Four of the IAV strains were isolated from mallard ducks and two were from marine mammals. We focused on 0 to 72 hpi since increases in IAV titers were observed over that period in the preliminary experiment (**Figure 2B**). We first determined kinetics of mean IAV titers in explants from trachea, bronchi, and lung from all rhesus macaques considered together (**Figure 3A-C**). Mean IAV infection kinetics increased from 0 to 72 hpi in all 3 explant tissues and reached highest levels at 72 hpi for most strains. Slower kinetics and lower peak titers by 10^{2-3} PFU/explant were observed in lungs compared to trachea and bronchi for most IAV strains. The mean area under the curve (AUC) was significantly higher for H3N8 and H7N5 strains compared to H1N1 and H5N2 strains in trachea and bronchi and trended higher in the lung, although not significantly (**Figure 3D**). Infection kinetics in explants from a representative rhesus macaque (M15) are shown in detail (**Figure S1**) and parallel strain differences observed in explants from the mean of all 10 animals. Infection kinetics in individual rhesus macaques over time (**Figure 4A**) also reveal the pattern of lower titers in the lung compared to trachea or bronchi. Together, these results show that multiple IAV subtypes infect respiratory tract explants from rhesus macaques with variable kinetics and peak titers.

Marine mammals: We next examined whether respiratory tract explants from marine mammals are susceptible to infection with the same IAV strains used to infect rhesus macaques. Explant tissues from California sea lions (N=11) and Northern elephant seals (N=2) were obtained from The Marine Mammal Center in Sausalito, CA. Marine mammals were mostly male ranging in age from yearling to subadult (**Table 2**). The causes of death varied and

were sometimes ascribed to an infectious or toxic etiology, but were not typically due to respiratory disease. All California sea lions used in this study had a mild burden of a lung worm, *Parafilaroides decorus*, which is found as a normal occurrence in healthy animals (36). As in rhesus macaques, IAV infection kinetics for most strains increased in California sea lions from 0 to 72 hpi in all 3 tissues and reached highest levels at 72 hpi for most strains (**Figure 3E-G**). Similar to rhesus macaques, the mean area under the curve (AUC) was significantly higher for H3N8 and H7N5 strains compared to H1N1 and H5N2 strains in trachea and bronchi while the AUC in lung explants from sea lions was only higher for H7N5 (**Figure 3H**). Detailed data (**Figure S2**) from 1 representative California sea lion (SL12) paralleled patterns from the mean of all 11 animals. Infection kinetics in individual marine mammals over time (**Figure 4B**) showed higher titers in the bronchi relative to trachea or lung. Contrary to our expectation that IAV of marine mammal origin would produce high titers in marine mammal explants, the strain from an elephant seal (ES/H1N1) produced lower and slower kinetics (**Figure 3E-G, 4B**) than many of the strains isolated from mallards or the harbor seal. These results show that, similar to rhesus macaques, multiple IAV subtypes infect respiratory tract explants from marine mammals with variable kinetics and peak titers. To further determine whether the differences in mean IAV kinetics were supported statistically over time, we examined the IAV infection dynamics in 24 hour windows.

IAV Kinetics Over Time: We tested whether explants inoculated with different IAV strains experience different mean changes in titer from 1 to 72 hpi. Considering all 3 tissue types together, the $\log_{10}$ change in viral titer was calculated for three time frames: 1 versus 24, 1 versus 48, and 1 versus 72 hpi for rhesus macaques and California sea lions (**Supplemental Table 1**). Northern elephant seals were not included in analyses since explants from only two animals were available, although they produced infectious IAV after inoculation with some strains (**Figure 4B**). Infection kinetics of the six IAV strains differed for each time frame considered. In rhesus macaques, mean titer changes for HS/H3N8, m/H3N8, and m/H7N5 did not differ significantly from each other over any of the time frames. m/H1N1 and mH5/N2 did not differ significantly from each other over any of the time frames but were different from HS/H3N8, m/H3N8 and m/H7N5. By contrast, the change in ES/H1N1 viral titers significantly differed from other all strains except for m/H1N1 from 1 to 48 hpi. In California sea lions, HS/H3N8 and m/H7N5 shared similar mean changes in $\log_{10}$ titers in all time frames. For m/H1N1 and HS/H3N8, the mean change in $\log_{10}$ titers did not vary significantly from 1 to 24 hpi but did vary from 1 to 48 and 1 to 72 hpi. The mean change in $\log_{10}$ viral titers between m/H1N1 and m/H7N5 were only different from 1 to 48 hpi and m/H5N2 and m/H7N5 differed from 1 to 48 and 1 to 72 hpi. These results show that mean changes in IAV titers over 24 hour

windows in respiratory tract explants from both rhesus macaques and California sea lions vary with IAV strain.

IAV Kinetics by Tissue: To examine whether tissue type associated with IAV titer, we analyzed all 6 IAV strains together (**Supplemental Table 2**). Infection kinetics in bronchi and trachea from rhesus macaques were significantly higher than in the lung over all 24 hour windows from 1 to 72 hpi. In California sea lions, infection kinetics in bronchi and trachea were significantly higher than in the lung at 24 hpi, while infection kinetics in bronchi were significantly higher than in the trachea and lung at 48 and 72 hpi. Together, these data support tissue-specific IAV infectivity, where bronchi and trachea explants from both species support production of higher IAV titers than lungs.

IAV Kinetics by Species: To evaluate whether species associates with infection kinetics for the 6 IAV strains, we compared changes in mean $\log_{10}$ titer between rhesus macaque and California sea lion explants (**Supplemental Table 3**). The mean change in titer of both H3N8 strains and m/H7N5 was significantly higher in trachea at all time points and in bronchi to 48 hpi in rhesus macaques compared to California sea lions. Changes in mean $\log_{10}$ titers for m/H3N8 in the lung from 1 to 48 and 1 to 72 hpi were higher in rhesus macaques compared to California sea lions. Together these data show that rhesus macaque explants produce higher titers compared to California sea lions for most IAV strains used here.

Cellular tropism of influenza A virus in rhesus macaque explants

We used immunohistochemistry to assess the cellular tropism of IAV in rhesus macaque and California sea lion respiratory tissue explants. (**Figure 5**, **Supplemental Table 4)**. At least 22 sections from each tissue type for 2 rhesus macaques (M11 and M13) and at least 56 sections from each tissue type for 2 California sea lions (SL08 and SL12) were evaluated. All examined sections exhibited variable degrees of nonspecific cytoplasmic, membranous and/or background staining; as such, only cells with strong nuclear immunoreactivity were considered positive. For all explants from both species and all IAV subtypes, positive staining for viral nucleoprotein was limited to epithelial cells of the trachea and bronchi; representative slides are shown (**Figure 5A-D**). Extensive sloughing of the bronchiolar epithelium beginning 24 hpi precluded assessment of this cell population for nuclear immunoreactivity. Pneumocytes within the lung were IAV negative. Infection was primarily localized to apical epithelial cells, particularly tracheal and bronchial ciliated columnar cells and goblet cells, while basal cells were largely spared. While there was variability between explants from the two rhesus macaques, explants infected with H3N8 strains exhibited higher relative proportions of positive tracheal and bronchial epithelial cells at 24 and 48 hpi, even though IAV titers for all strains except

ES/H1N1 exceeded 10^4 PFU/explant (**Figure 4A**).The explants from M11 infected with m/H7N5 exhibited the largest variation in relative proportion of positive cells between 24 and 48 hpi. The number of infected respiratory epithelial cells generally increased between 24 and 48 hpi, which is consistent with infection kinetics where IAV titers increased during that period. While positive nuclei were less frequent within California sea lion explants, those infected with H3N8 strains also exhibited higher relative proportions of positive tracheal and bronchial epithelial cells at 24 and 48 hpi, which is consistent with data from rhesus macaques. These results demonstrate that IAV infects the apical epithelial cells of upper respiratory tract explants in rhesus macaques and California sea lions.

Genetic changes in influenza A viruses sequenced from explants

IAV genomes in inoculated explants from 2 rhesus macaques, 3 California sea lions, and 1 Northern elephant seal were compared to sequences in strains used as inocula (**Supplemental Table 5**). Sequence comparisons showed that all genomes from rhesus macaque explants were 100% identical at the consensus level (mutations occurring on 50% or more of viral RNAs) to their corresponding inoculum (data not shown). Six nonsynonymous nucleotide substitutions in the HA, NA, and PA genes were detected in California sea lion and Northern elephant seal explants inoculated with different IAV subtypes (**Supplemental Table 6**). Inocula contained a mixture of bases including the mutant nucleotide at each of these loci, indicating that none of the mutations developed *de novo* in explants (data not shown). One synonymous nucleotide substitution, PB2 1368 in m/H7N5, was detected in bronchi from all 3 California sea lions at 48 and 72 hpi. The nucleotide affecting this substitution was present at a minority frequency (41%) in the inoculum, indicating that it did not develop *de novo* but increased to consensus frequency in explants by 48 hpi (data not shown). Together these data show that no *de novo* IAV mutations were detected in any strain during *ex vivo* respiratory tract explant infection from selected rhesus macaques and marine mammals.

SARS-CoV-2 infects rhesus macaque respiratory tract explants

Using African green monkey kidney (Vero) cells, we first characterized infection kinetics (**Figure 6A**) at multiple MOIs for a SARS-CoV-2 strain that was originally isolated from a patient at the University of California, Davis Medical Center and passaged in Vero cells. Titers increased over time and were significantly higher 8 hpi at a MOI of 1 relative to the lower MOIs tested ($p<0.001$, repeated measures 2 way ANOVA). Peak titers at all 3 MOIs at 48 hpi were not significantly different ($p>0.05$, repeated measures 2 way ANOVA) and approached 10^6 PFU/ml. At 24 hpi, the majority of cultured Vero-E6 cells inoculated at an MOI of 0.1 were infected based on staining with an anti-SARS-CoV-2 nucleocapsid antibody (**Figure 6B**). Labeling patterns were similar to those previously described with SARS-CoV-2 (37), and manifest as punctate reactivity within the cytoplasm and an eccentric halo around the nucleus, which, based on the known replication cycle and assembly of coronaviruses,

corresponds to association with endoplasmic reticulum, which is contiguous with the nuclear envelope. We expanded the explant system with a similar approach as for IAV (**Figure 6C**) to characterize SARS-CoV-2 susceptibility and infection dynamics in respiratory tract explants from 2 rhesus macaques by inoculating $1X10^4$ PFU of SARS-CoV-2 into trachea, lung, kidney, and liver, where the latter 2 tissues were included as non-target controls. Similar to IAV, SARS-CoV-2 infected the trachea of both macaques and the lung of a 2.3 year-old female (M31), but no infectious virus was detected in the lung of a 4 month-old female macaque 24 hpi (M32) (**Figure 6D**). SARS-CoV-2 infected the kidney but not the liver from both animals. Immunofluorescence of infected lung explants 48 hpi using an antibody directed against SARS-CoV-2 mirrored infectious virus detected by titrations. Viral antigen was detectable in the lung explant of M31 (**Figure 6E**) but not in an explant from M32 (not shown). Antibody reactive cells were elongate and lined alveolar spaces. Scattered cells present within the alveolar lumen were presumably degenerate cytolyzed epithelial cells based on the lack of nuclear detail, as evidenced by a low DAPI signal. These results demonstrate that rhesus macaque respiratory tract tissues and kidney explants support productive infection by SARS-CoV-2.

Discussion

We adapted an *ex vivo* respiratory tract infection model to study susceptibility and to define comparative infection kinetics of IAV in rhesus macaques and marine mammals. We observed that IAV exhibits temporal, subtype- and species-dependent infection kinetics. Although the relative infection kinetics for the six strains was similar for rhesus macaques and California sea lions, similar patterns were not observed in MDCK cells. This suggests that immortalized cell lines may not represent infection phenotypes *in vivo*, further underscoring the use of *ex vivo* systems. Our pilot studies also show that SARS-CoV-2 infects *ex vivo* rhesus macaque explants.

E*x vivo* respiratory tract models have been used for studying respiratory pathogens of humans, swine, bovines, canines, and equines (23, 25–28, 38–40). *Ex vivo* cultures of respiratory tissues provide a close resemblance to the respiratory tract *in vivo* by: 1) shared polarity, where the basolateral surface is exposed to culture medium and the apical cell surface is exposed to air, 2) shared cell positioning *in situ* which could maintain virus receptor distribution, 3) possession of multiple cell types and states of differentiation, 4) maintenance of the three dimensional integrity and architecture of a tissue, unlike cell monocultures, and 5) ciliary activity to maintain mucociliary clearance. Given these similarities to living IAV hosts, explants are valuable tools for assessing host susceptibility, infection kinetics, and pathogenesis of respiratory pathogens. The *ex vivo* systems also better assess infectivity compared to cell

monoculture binding assays that only measure virus-receptor affinity (25, 27). In addition, tissues collected from a single animal can be divided into pieces and used to compare relative infectivity of different viral strains while holding the host constant. Last, use of explants from animals euthanized for other reasons reduced the number of animals used in research, following the principles of reduction, replacement, and refinement.

Limitations of the *ex vivo* approach include restricted availability of tissues, short periods of viability, and inter-animal variability in IAV susceptibility. The absence of a blood supply also constitutes a weakness of the *ex vivo* respiratory explant system since recruitment of immune cells to the infection site cannot occur. However, such a pitfall might be co-opted in future studies to understand the effects of innate and intrinsic immunity without immune cell influx.

Lower IAV titers in *ex vivo rhesus* macaque and marine mammal lungs relative to trachea and bronchi support the upper respiratory tract is the primary site of virus infection with the virus strains used in this study. The ability of IAV to produce higher titers in the upper respiratory tract may reflect adaptation of the virus to best infect cell targets in closest anatomic proximity to its entry point and shedding site, the respiratory mucosa.

The infection kinetics of H3N8 and H7N5 strains in rhesus macaque and California sea lion respiratory tract explant tissues were superior to H1N1 and H5N2 strains, although all share similar passage histories. A similar pattern of differential strain infectivity was observed in swine, where human H3N2 infected explants more efficiently than H1N1 (41), and in humans, where H7N9 achieved higher titers than high pathogenic H5N1 and H5N6 (27). In spite of the different infection kinetics across strains, the 6 strains used here, representing 4 IAV subtypes, productively infected at least one explant type for both species. These data suggest that any of these subtypes could also infect marine mammals in the wild, consistent with serologic data showing exposure to many subtypes (13–16, 18, 19).

The observation that SARS-CoV-2 infects *ex vivo* rhesus macaque explants parallels findings from *ex vivo* lungs from human donors whose lungs were removed due to tumors or from patients undergoing elective surgery (28, 42). Infection kinetics increased from 2 to 48 hpi in explants and increases in virus titers were greater in explants inoculated with SARS-CoV-2 compared to SARS-CoV. Given similar findings from our studies with a limited number of rhesus macaque explants infected with SARS-CoV-2, *ex vivo* respiratory tract explants represent an important tool to employ for SARS-CoV-2 to fully define infection dynamics and pathogenesis, host innate responses, viral genetic determinants of infection, and antiviral treatments.

DATA AVAILABILITY

Sequencing data are available at the CEIRS Data Processing and Coordinating Center (DPCC) Project Identifier: SP4-Boyce_5004 and Submission_ID: 1136547734004. GenBank accession numbers will be posted when available.

ACKNOWLEDGEMENTS

We are immensely grateful for our collaborators at The Marine Mammal Center, we thank the veterinary and research staff for coordinating the collection and transfer of fresh tissue samples to our laboratory. Sample possession was granted by The National Oceanic and Atmospheric Administration National Marine Fisheries Service Letter of Authorization.

FUNDING ACKNOWLEDGEMENTS

Funding support was provided by NIH NIAID #HHSN272201400008C to WB and LLC and from the University of California, Davis Office of Research to PAP and HL. EEB was supported by a Comparative Medical Science Training Program T32 fellowship # OD011147. We thank Kathy West at the California National Primate Research Center for generating the rhesus macaque image used in figures and Ana L. Ramirez for generating the other images used in figures.

COMPETING INTERESTS

The authors declare that there are no competing interests.

AUTHOR CONTRIBUTIONS

Conceptualization: HL, MP, WB, LLC, Methodology: HL, CMW, LLC, BH, Investigation: HL, MP, CMW, OG-V, AMA, EEB, ZMM, KMH, KJ, PAP, ZK, DK. Writing-original draft: HL, LLC. Writing-review and editing: HL, CMW, MP, EEB, ZMM, HB, BH, KMH, WB, PAP, LLC. Visualization: HL, CMW, EEB, PAP, KJ, LLC. Supervision and project administration: WB, HB, LLC. Funding acquisition: WB, HL, PAP, LLC.

REFERENCES

1. Krammer F, Smith GJD, Fouchier RAM, Peiris M, Kedzierska K, Doherty PC, Palese P, Shaw ML, Treanor J, Webster RG, García-Sastre A. 2018. Influenza. Nat Rev Dis Prim. 28;4(1):3.
2. Landolt GA, Olsen CW. 2007. Up to new tricks - a review of cross-species transmission of influenza A viruses. Anim Health Res Rev. 8(1):1-21.
3. Taubenberger JK, Kash JC. 2010. Influenza virus evolution, host adaptation, and pandemic

formation. Cell Host Microbe. 25;7(6):440-51.

4. Goldstein T, Mena I, Anthony SJ, Medina R, Robinson PW, Greig DJ, Costa DP, Lipkin WI, Garcia-Sastre A, Boyce WM. 2013. Pandemic H1N1 Influenza Isolated from Free-Ranging Northern Elephant Seals in 2010 off the Central California Coast. PLoS One. 15;8(5):e62259.

5. Karlsson EA, Ip HS, Hall JS, Yoon SW, Johnson J, Beck MA, Webby RJ, Schultz-Cherry S. 2014. Respiratory transmission of an avian H3N8 influenza virus isolated from a harbour seal. Nat Commun. 3;5:4791.

6. Reperant LA, Kuiken T, Osterhaus ADME. 2012. Adaptive pathways of zoonotic influenza viruses: From exposure to establishment in humans. Vaccine. 30(30):4419-34.

7. Kaplan BS, Webby RJ. 2013. The avian and mammalian host range of highly pathogenic avian H5N1 influenza. Virus Res.178(1):3-11.

8. Sikkema RS, Freidl GS, de Bruin E, Koopmans M. 2016. Weighing serological evidence of human exposure to animal influenza viruses − A literature review. Eurosurveillance. 21(44):30388.

9. Suttie A, Deng YM, Greenhill AR, Dussart P, Horwood PF, Karlsson EA. 2019. Inventory of molecular markers affecting biological characteristics of avian influenza A viruses. Virus Genes. 55(6):739-768.

10. Lang G, Gagnon A, Geraci JR. 1981. Isolation of an influenza A virus from seals. Arch Virol. 68(3-4):189-95.

11. Webster RG, Hinshaw VS, Bean WJ, Van Wyke KL, Geraci JR, St. Aubin DJ, Petursson G. 1981. Characterization of an influenza A virus from seals. Virology. 113(2):712-24.

12. Geraci JR, Aubin DJS, Barker IK, Webster RG, Hinshaw VS, Bean WJ, Ruhnke HL, Prescott JH, Early G, Baker AS, Madoff S, Schooley RT. 1982. Mass mortality of harbor seals: Pneumonia associated with influenza A virus. Science. 215(4536):1129-31

13. Ohishi K, Kishida N, Ninomiya A, Kida H, Takada Y, Miyazaki N, Boltonov AN, Maruyama T. 2004. Antibodies to human-related H3 influenza A virus in Baikal seals (*Phoca sibirica*) and ringed seals (*Phoca hispida*) in Russia. Microbiol Immunol. 48(11):905-9

14. Fereidouni S, Munoz O, Von Dobschuetz S, De Nardi M. 2014. Influenza virus infection of marine mammals. Ecohealth. 13(1):161-70

15. Puryear WB, Keogh M, Hill N, Moxley J, Josephson E, Davis KR, Bandoro C, Lidgard D, Bogomolni A, Levin M, Lang S, Hammill M, Bowen D, Johnston DW, Romano T, Waring G, Runstadler J. 2016. Prevalence of influenza A virus in live-captured North Atlantic gray seals: A possible wild reservoir. Emerg Microbes Infect. 5(8):e81.

16. Stuen S, Have P, Osterhaus AD, Arnemo JM, Moustgaard A. 1994. Serological investigation of virus infections in harp seals (*Phoca groenlandica*) and hooded seals (*Cystophora cristata*). Vet Rec. 134(19):502-3.

17. Nielsen O, Clavijo A, Boughen JA. 2001. Serologic evidence of influenza A infection in marine mammals of Arctic Canada. J Wildl Dis. 37(4):820-5.
18. Greig DJ, Gulland FMD, Smith WA, Conrad PA, Field CL, Fleetwood M, Harvey JT, Ip HS, Jang S, Packham A, Wheeler E, Hall AJ. 2014. Surveillance for zoonotic and selected pathogens in harbor seals *Phoca vitulina* from central California. Dis Aquat Organ. 111(2):93-106
19. Danner GR, Mcgregor MW, Zarnke RL, Olsen CW. 1998. Serologic evidence of influenza virus infection in a ringed seal (*Phoca hispida*) from Alaska. Mar Mammal Sci. 14:380–384.
20. Venkatesh D, Bianco C, Núñez A, Collins R, Thorpe D, Reid SM, Brookes SM, Essen S, McGinn N, Seekings J, Cooper J, Brown IH, Lewis NS. 2020. Detection of H3N8 influenza A virus with multiple mammalian-adaptive mutations in a rescued Grey seal (*Halichoerus grypus*) pup. Virus Evol. 6(1):veaa016.
21. Capuano AM, Miller M, Stallknecht DE, Moriarty M, Plancarte M, Dodd E, Batac F, Boyce WM. 2017. Serologic detection of subtype-specific antibodies to influenza A viruses in southern sea otters (*Enhydra lutris nereis*). J Wildl Dis. 53(4):906-910
22. Ramey AM, Hill NJ, Cline T, Plancarte M, De La Cruz S, Casazza ML, Ackerman JT, Fleskes JP, Vickers TW, Reeves AB, Gulland F, Fontaine C, Prosser DJ, Runstadler JA, Boyce WM. 2017. Surveillance for highly pathogenic influenza A viruses in California during 2014-2015 provides insights into viral evolutionary pathways and the spatiotemporal extent of viruses in the Pacific Americas Flyway. Emerg Microbes Infect. 6(9):e80.
23. Nunes SF, Murcia PR, Tiley LS, Brown IH, Tucker AW, Maskell DJ, Wood JLN. 2010. An *ex vivo* swine tracheal organ culture for the study of influenza infection. Influenza Other Respi Viruses. 4(1):7-15.
24. Löndt BZ, Brookes SM, Nash BJ, Núñez A, Stagg DA, Brown IH. 2013. The infectivity of pandemic 2009 H1N1 and avian influenza viruses for pigs: An assessment by *ex vivo* respiratory tract organ culture. Influenza Other Respi Viruses. 7(3):393-402.
25. Chan RWY, Chan MCW, Nicholls JM, Malik Peiris JS. 2013. Use of *ex vivo* and *in vitro* cultures of the human respiratory tract to study the tropism and host responses of highly pathogenic avian influenza A (H5N1) and other influenza viruses. Virus Res. 178(1):133-45.
26. Nicholas B, Staples KJ, Moese S, Meldrum E, Ward J, Dennison P, Havelock T, Hinks TSC, Amer K, Woo E, Chamberlain M, Singh N, North M, Pink S, Wilkinson TMA, Djukanović R. 2015. A Novel Lung Explant Model for the *Ex Vivo* Study of Efficacy and Mechanisms of Anti-Influenza Drugs. J Immunol. 194(12):6144-54.
27. Hui KPY, Ching RHH, Chan SKH, Nicholls JM, Sachs N, Clevers H, Peiris JSM, Chan MCW. 2018. Tropism, replication competence, and innate immune responses of influenza virus: an analysis of human airway organoids and *ex-vivo* bronchus cultures. Lancet Respir Med.

6(11):846-854.

28. Hui KPY, Cheung MC, Perera RAPM, Ng KC, Bui CHT, Ho JCW, Ng MMT, Kuok DIT, Shih KC, Tsao SW, Poon LLM, Peiris M, Nicholls JM, Chan MCW. 2020. Tropism, replication competence, and innate immune responses of the coronavirus SARS-CoV-2 in human respiratory tract and conjunctiva: an analysis in *ex-vivo* and i*n-vitro* cultures. Lancet Respir Med 8:687–695.

29. Munster VJ, Feldmann F, Williamson BN, van Doremalen N, Pérez-Pérez L, Schulz J, Meade-White K, Okumura A, Callison J, Brumbaugh B, Avanzato VA, Rosenke R, Hanley PW, Saturday G, Scott D, Fischer ER, de Wit E. 2020. Respiratory disease in rhesus macaques inoculated with SARS-CoV-2. Nature. 585(7824):268-272.

30. Chandrashekar A, Liu J, Martinot AJ, McMahan K, Mercado NB, Peter L, Tostanoski LH, Yu J, Maliga Z, Nekorchuk M, Busman-Sahay K, Terry M, Wrijil LM, Ducat S, Martinez DR, Atyeo C, Fischinger S, Burke JS, Slein MD, Pessaint L, Van Ry A, Greenhouse J, Taylor T, Blade K, Cook A, Finneyfrock B, Brown R, Teow E, Velasco J, Zahn R, Wegmann F, Abbink P, Bondzie EA, Dagotto G, Gebre MS, He X, Jacob-Dolan C, Kordana N, Li Z, Lifton MA, Mahrokhian SH, Maxfield LF, Nityanandam R, Nkolola JP, Schmidt AG, Miller AD, Baric RS, Alter G, Sorger PK, Estes JD, Andersen H, Lewis MG, Barouch DH. 2020. SARS-CoV-2 infection protects against rechallenge in rhesus macaques. Science. 369(6505):812-817.

31. Deng W, Bao L, Liu J, Xiao C, Liu J, Xue J, Lv Q, Qi F, Gao H, Yu P, Xu Y, Qu Y, Li F, Xiang Z, Yu H, Gong S, Liu M, Wang G, Wang S, Song Z, Liu Y, Zhao W, Han Y, Zhao L, Liu X, Wei Q, Qin C. 2020. Primary exposure to SARS-CoV-2 protects against reinfection in rhesus macaques. Science. 369(6505):818-823.

32. Weiss CM, Coffey LL. Engineering a fidelity-variant live-attenuated vaccine for chikungunya virus. 2020. npj Vaccines 1–14. In press.

33. Mena I, Nelson MI, Quezada-Monroy F, Dutta J, Cortes-Fernández R, Lara-Puente JH, Castro-Peralta F, Cunha LF, Trovão NS, Lozano-Dubernard B, Rambaut A, Van Bakel H, García-Sastre A. 2016. Origins of the 2009 H1N1 influenza pandemic in swine in Mexico. Elife. 5:e16777.

34. Venkatesh D, Poen MJ, Bestebroer TM, Scheuer RD, Vuong O, Chkhaidze M, Machablishvili A, Mamuchadze J, Ninua L, Fedorova NB, Halpin RA, Lin X, Ransier A, Stockwell TB, Wentworth DE, Kriti D, Dutta J, van Bakel H, Puranik A, Slomka MJ, Essen S, Brown IH, Fouchier RAM, Lewis NS. 2018. Avian Influenza Viruses in Wild Birds: Virus Evolution in a Multihost Ecosystem. J Virol. 92(15):e00433-18.

35. R Core Team. 2020. R: A language and environment for statistical computing. R Foundation for Statistical Computing, Vienna, Austria. https://www.R-project.org/.

36. Greig DJ, Gulland FMD, Kreuder C. 2005. A Decade of Live California Sea Lion (*Zalophus*

californianus) Strandings Along the Central California Coast: Causes and Trends, 1991-2000. Aquat Mamm.31(1):11-21.

37. Ogando NS, Dalebout TJ, Zevenhoven-Dobbe JC, Limpens RWAL, van der Meer Y, Caly L, Druce J, de Vries JJC, Kikkert M, Bárcena M, Sidorov I, Snijder EJ. 2020. SARS-coronavirus-2 replication in Vero E6 cells: replication kinetics, rapid adaptation and cytopathology. J Gen Virol. 101(9):925-940.

38. Vandekerckhove A, Glorieux S, Broeck W Van den, Gryspeerdt A, van der Meulen KM, Nauwynck HJ. 2009. *In vitro* culture of equine respiratory mucosa explants. Vet J. 181(3):280-7.

39. Priestnall SL, Mitchell JA, Brooks HW, Brownlie J, Erles K. 2009. Quantification of mRNA encoding cytokines and chemokines and assessment of ciliary function in canine tracheal epithelium during infection with canine respiratory coronavirus (CRCoV). Vet Immunol Immunopathol. 127(1-2):38-46.

40. Niesalla HS, Dale A, Slater JD, Scholes SFE, Archer J, Maskell DJ, Tucker AW. 2009. Critical assessment of an in vitro bovine respiratory organ culture system: A model of bovine herpesvirus-1 infection. J Virol Methods. 158(1-2):123-9.

41. Van Poucke SGM, Nicholls JM, Nauwynck HJ, Van Reeth K. 2010. Replication of avian, human and swine influenza viruses in porcine respiratory explants and association with sialic acid distribution. Virol J. 7:38.

42. Chu H, Chan JFW, Wang Y, Yuen TTT, Chai Y, Hou Y, Shuai H, Yang D, Hu B, Huang X, Zhang X, Cai JP, Zhou J, Yuan S, Kok KH, To KKW, Chan IHY, Zhang AJ, Sit KY, Au WK, Yuen KY. 2020. Comparative replication and immune activation profiles of SARS-CoV-2 and SARS-CoV in human lungs: an ex vivo study with implications for the pathogenesis of COVID-19. Clin Infect Dis. 71(6):1400-1409

744
745
746
747
748
749
750
751
752
753

Table 1. IAV or SARS-CoV-2 strains used for explant infection experiments. ES is elephant seal, HS is harbor seal, m is mallard. N/A indicates strain was isolated at UC Davis and first described in this study. MDCK is Madin-Darby canine kidney cell. n/a is not applicable.

Virus ID	Strain name	Subtype	Passage number	MDCK or Vero E6 titer (PFU/ml)	GenBank Accession number	Reference
ES/H1N1	A/Elephant seal/California/1/2010	H1N1	p4	$1.3x10^8$	JX865419-JX865426	Goldstein et al. 2013 (1)
HS/H3N8	A/harbor seal/New Hampshire/179629/2011	H3N8	p3	$1.8x10^6$	KJ467564-KJ467571	Karlsson et al. 2014 (2)
m/H3N8	A/mallard/California/1475/2010	H3N8	p2	$6x10^6$	CY120501-CY120508	N/A
m/H1N1	A/mallard/California/3134/2010	H1N1	p2	$4x10^7$	CY120611-CY120618	N/A
m/H5N2	A/mallard/California/2396/2010	H5N2	p2	$4x10^7$	CY120587-CY120594	N/A
m/H7N5	A/mallard/California/1390/2010	H7N5	p2	$1x10^7$	CY120555-CY120562	N/A
SARS-CoV-2	human/USA/CA-CZB-59X001/2020	n/a	p2	2.2×10^7	MT394529	Deng et al. 2020 (3)

Table 2. Explant sources for IAV or SARS-CoV-2 *ex vivo* infection studies. For IAV studies, tissues were derived from 10 rhesus macaques (*Macaca mulatta*), 11 California sea lions (*Zalophus californianus*) and 2 northern elephant seals (*Mirounga angustirostris)*. For SARS-CoV-2 studies, tissues were derived from 2 rhesus macaques.

Virus	Animal	Species	Sex	Age	Reason for euthanasia
IAV	M12	*Macaca mulatta*	Male	1y	Chronic diarrhea
	M13	*Macaca mulatta*	Male	3y4m	Lameness due to trauma
	M15	*Macaca mulatta*	Male	4y5m	Severe leg trauma
	M16	*Macaca mulatta*	Male	3y6m	Chronic diarrhea
	M17	*Macaca mulatta*	Male	4y5m	Chronic diarrhea
	M11	*Macaca mulatta*	Female	5y11m	Chronic diarrhea
	M14	*Macaca mulatta*	Female	16y6m	Endometriosis
	M19	*Macaca mulatta*	Female	1y6m	Chronic diarrhea
	M21	*Macaca mulatta*	Female	4y	Severe leg trauma
	M20	*Macaca mulatta*	Female	3y11m	Liver amyloid, diarrhea, bloating
SARS-CoV-2	M31	*Macaca mulatta*	Female	2y3m	Chronic diarrhea, rectal prolapses
	M32	*Macaca mulatta*	Female	4m	Non-pathogenic diarrhea
IAV	SL01	*Zalophus californianus*	male	yearling	Malnourished, peritonitis
	SL02	*Zalophus californianus*	male	yearling	Leptospirosis, mild pneumonia
	SL03	*Zalophus californianus*	male	yearling	Leptospirosis
	SL04	*Zalophus californianus*	male	juvenile	Leptospirosis
	SL05	*Zalophus californianus*	male	subadult	Leptospirosis, seizures
	SL06	*Zalophus californianus*	male	subadult	Leptospirosis
	SL07	*Zalophus californianus*	male	subadult	Leptospirosis
	SL08	*Zalophus californianus*	male	yearling	Asphyxia
	SL13	*Zalophus californianus*	male	yearling	Domoic acid toxicity
	SL09	*Zalophus californianus*	female	adult	Domoic acid toxicity
	SL12	*Zalophus californianus*	female	adult	Septicemia
	ES10	*Mirounga angustirostris*	male	yearling	Tachypnea, tachycardia
	ES11	*Mirounga angustirostris*	male	weanling	Blindness; congenital defect

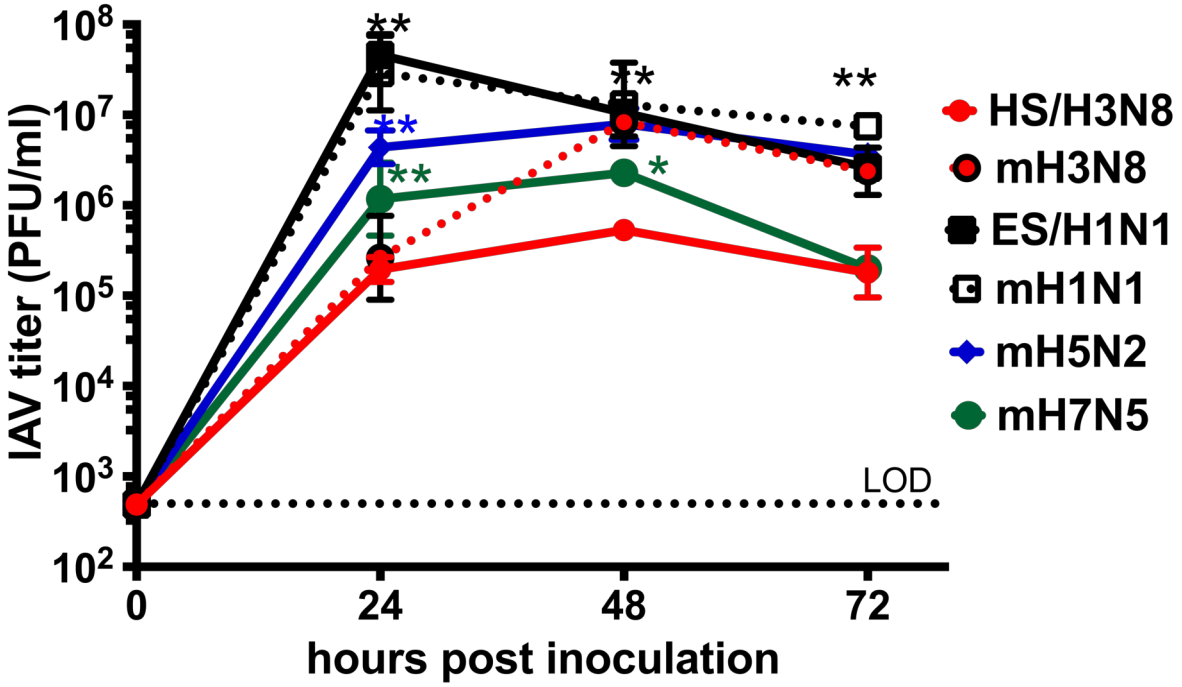

Figure 1. *In vitro* infection kinetics of 6 influenza A virus strains in Madin-Darby canine kidney cells. A MOI of 0.01 was used. The geometric mean virus titer from triplicate wells at each time point was plotted as PFU per milliliter ± geometric standard deviation. The dotted line represents the limit of detection (LOD) of 500 PFU/ml. Asterisks show comparisons of mean titers between HS/H3N8 and all other strains analyzed by two-way ANOVA of log transformed values where * is $p < 0.001$ and ** is $p < 0.0001$. Strain names refer to the original source of the virus isolate followed by the hemagglutinin and neuraminidase subtype. HS is harbor seal. m is mallard. ES is elephant seal.

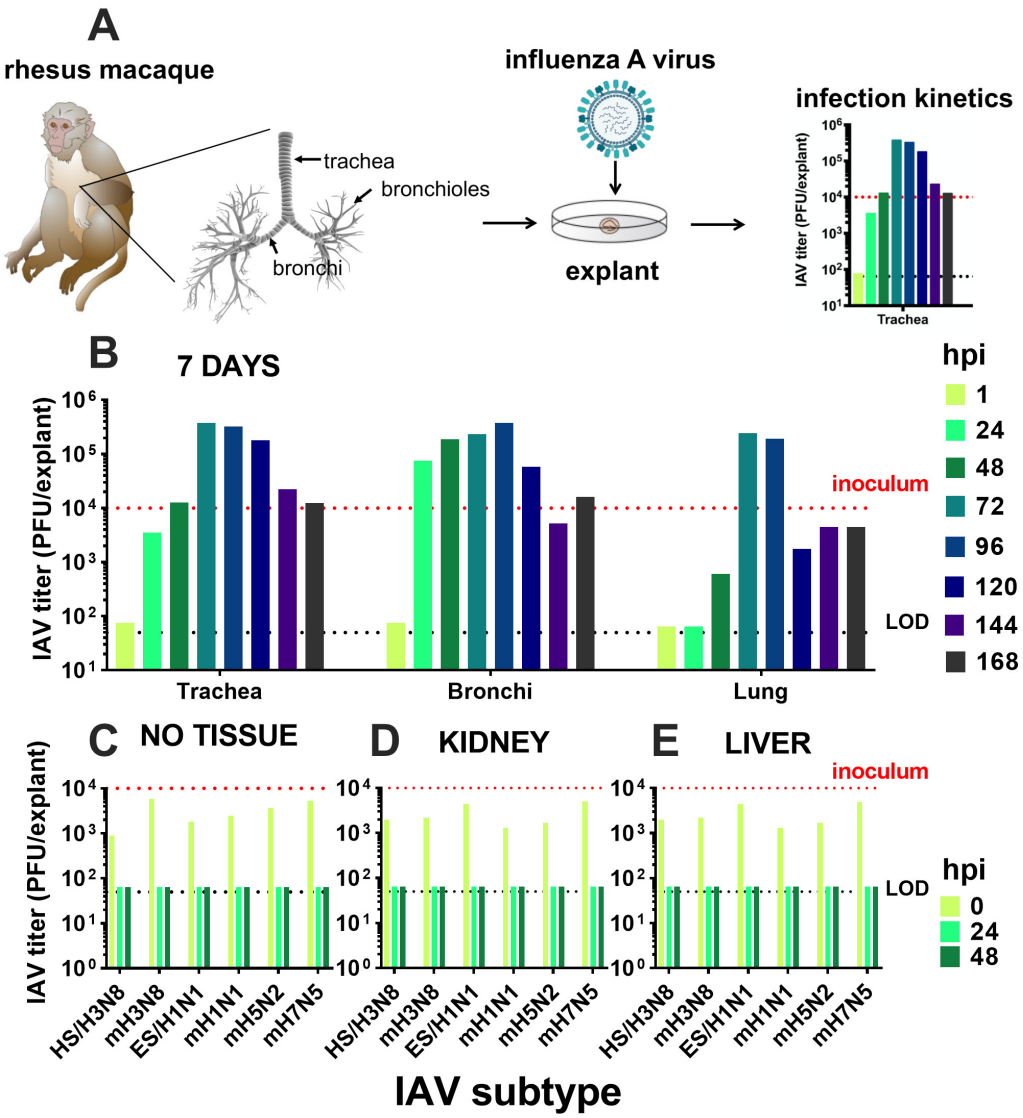

Figure 2 (A) Experimental design for *ex vivo* rhesus macaque respiratory tract explant inoculations with influenza A virus (IAV). **(B)** Seven day infection kinetics of IAV HS/H3N8 in explants from an 11 year old animal. **(C)** IAV titers in the absence of explants to evaluate stability of infectious virus from 0 to 48 hpi. IAV titers in kidney **(D)** and liver **(E)**, tissues that are not IAV targets from a 3.5 year old animal from 0 to 48 hpi. Each bar shows the measurement from a single explant. The dotted black line shows the limit of detection, 50 PFU/explant. The red line shows the inoculum. hpi is hours post inoculation. Strain names refer to the original source of the virus isolate followed by the hemagglutinin and neuraminidase subtype. HS is harbor seal. m is mallard. ES is elephant seal.

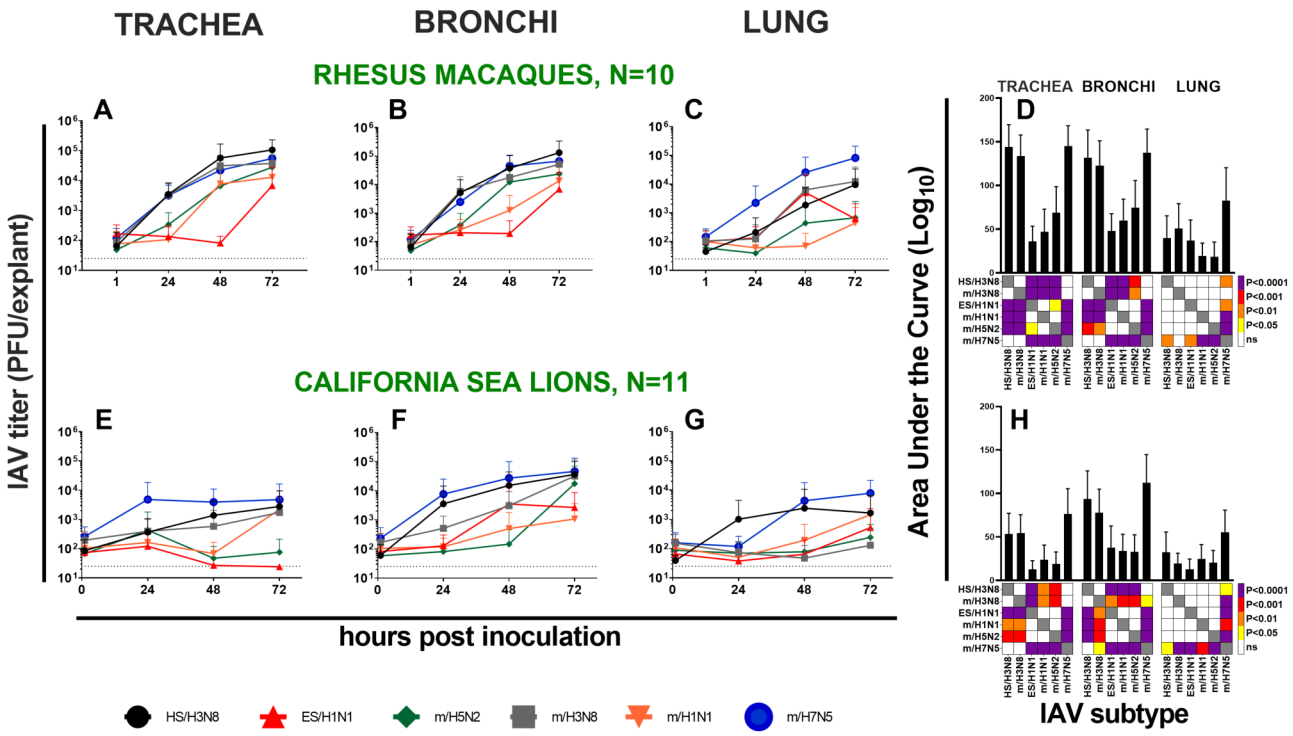

Figure 3: **Ex vivo influenza A virus infection kinetics.** Mean kinetics in 10 rhesus macaque (**A-C**) and 11 California sea lions (**E-G**) and areas under the infection curve (AUC) (**D, H**) in *ex vivo* respiratory tract trachea, bronchi, and lung explants. Error bars show standard deviations. The dotted black line shows the limit of detection, 50 PFU/explant. Colors in squares in D and H show differences in mean AUC by strain analyzed using one-way ANOVA tests where the darker the color, the smaller the p-value. Strain names refer to the original source of the virus isolate followed by the hemagglutinin and neuraminidase subtype. HS is harbor seal. m is mallard. ES is elephant seal.

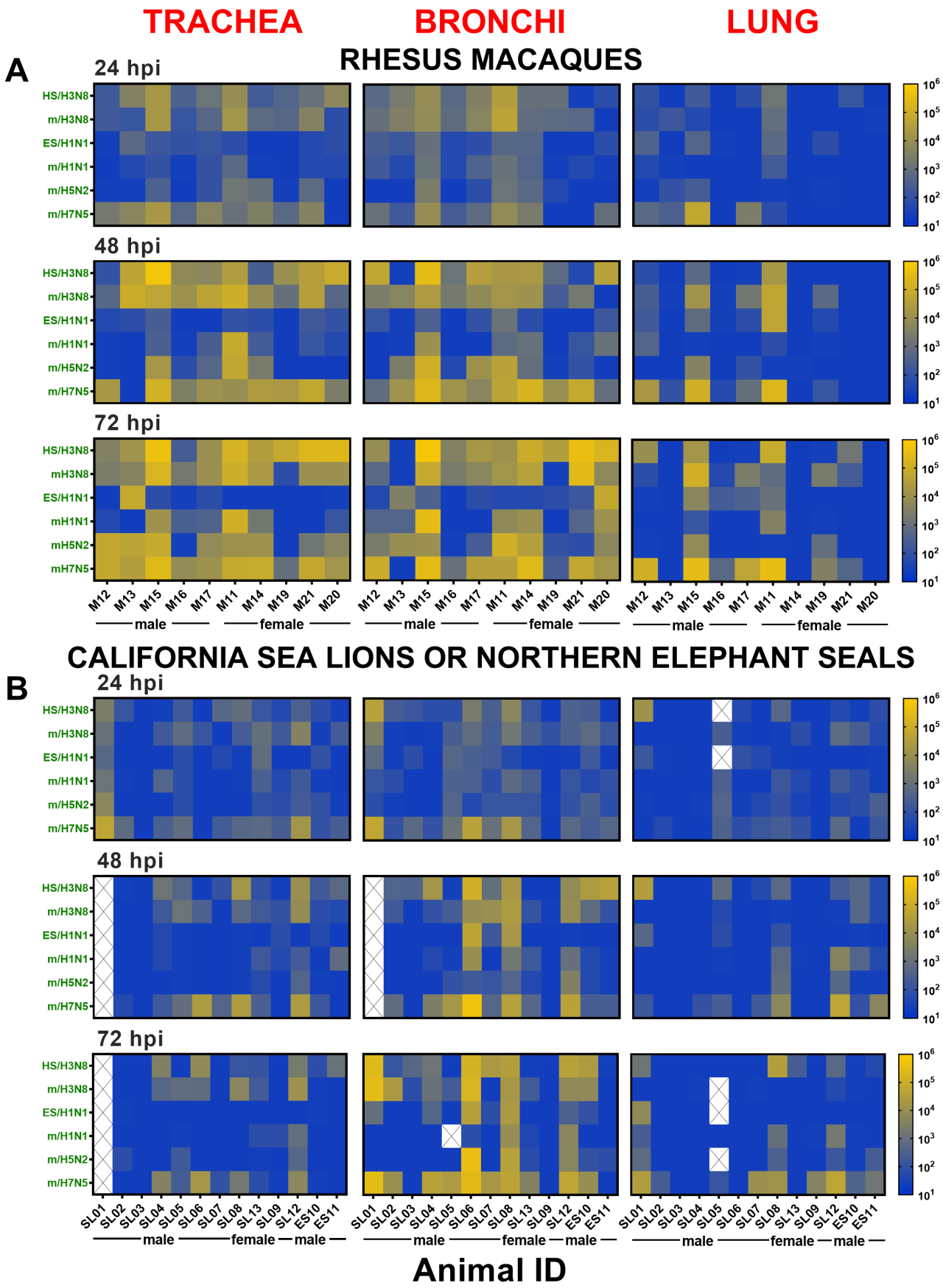

Figure 4. Comparison of *ex vivo* influenza A virus infection kinetics in respiratory tract explants from individual animals. (A) IAV titers in explants from 10 rhesus macaques and **(B)** 11 California sea lions and 2 Northern elephant seals inoculated with 1 x 10^4 PFU and 2 x 10^4 PFU of each of the 6 IAV strains over a 72 hour period. The kinetics of viral infection were determined by plaque assays of homogenized explants, where each square represents the titer from 10^1 (blue) to 10^6 (yellow) in PFU/explant. The limit of detection was 50 PFU/explant. Each explant was titrated once at 2-3 dilutions. Strain names refer to the original source of the virus isolate followed by the hemagglutinin and neuraminidase subtype (Table 1). HS is harbor seal. m is mallard. ES is elephant seal. Boxes with 'X' indicate the sample was not available for titration.

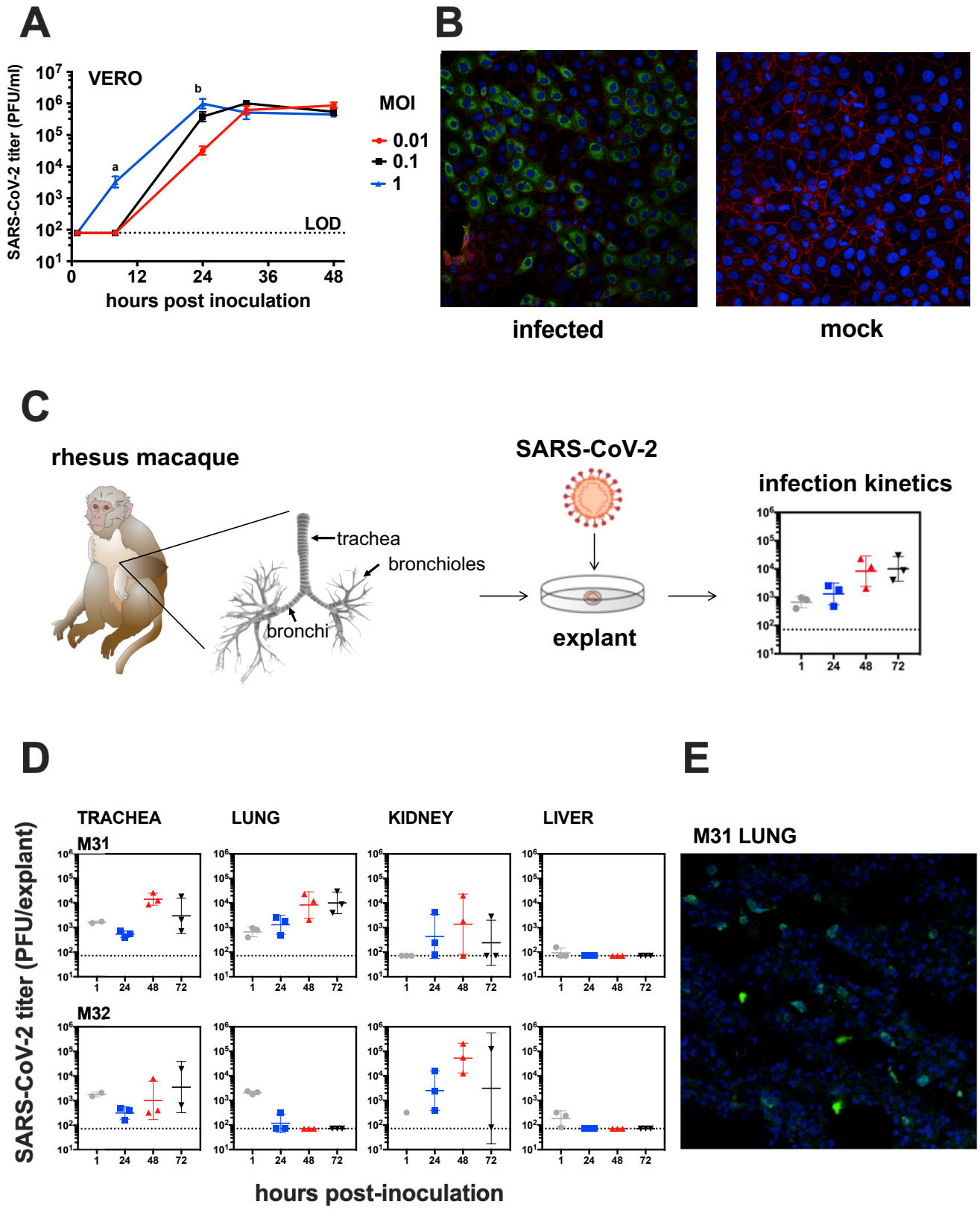

Figure 6: SARS-CoV-2 infection kinetics in Vero cells and ex vivo rhesus macaque respiratory tract explants. (A) *In vitro* infection kinetics of SARS-CoV-2 in Vero-E6 cells at

designated MOIs. The geometric mean virus titer from triplicate wells at each time point is plotted as PFU per milliliter ± geometric standard deviation. The dotted line represents the limit of detection (LOD) of 80 PFU/ml. a denotes that the mean titer for the MOI 1 wells was significantly different from the MOI 0.1 and 0.01 groups ($p<0.01$), b shows that the mean titer for the MOI 0.01 wells was significantly different from the MOI 0.1 and 1 groups ($p<0.01$). No symbol indicates that values for all 3 MOIS were not significantly different ($p>0.05$) Statistical tests were repeated measures 2 way ANOVAs. **(B)** Representative fields from a monolayer of Vero-E6 cells 24 hpi with SARS-CoV-2 at an MOI of 0.1 (green) or mock. Intact tight junctions are represented (red) by anti-ZO-1, and nuclear DNA stained with DAPI (blue). Magnification for both images is 20X. (**C**) Experimental design for *ex vivo* rhesus macaque respiratory tract explant inoculations with SARS-CoV-2. **(D)** SARS-CoV-2 infection kinetics in *ex vivo* explants from a 2.3 year-old female (M31) and a 4 month-old female (M32) rhesus macaque inoculated with 1×10^4 PFU SARS-CoV-2. The kinetics of viral infection were determined by plaque assays of homogenized explants, where each symbol represents the titer from one explant. The limit of detection was 80 PFU/explant; samples with no detectable virus are reported at the LOD. Each explant was titrated once at 4 dilutions. **(E)** Immunofluorescence image of a lung explant (M32) 48 hpi magnified 20 times showing alveolar interstitium and highlighting SARS-CoV-2 (green) present in the cytoplasm of multifocal cells that line alveolar spaces. A few cells that are present within the alveolar lumen lack formed nuclei and are more brightly stained, this may results from cell cytolysis caused by viral infection. DAPI counterstain reveals nuclei.

SUPPLEMENTAL FIGURES

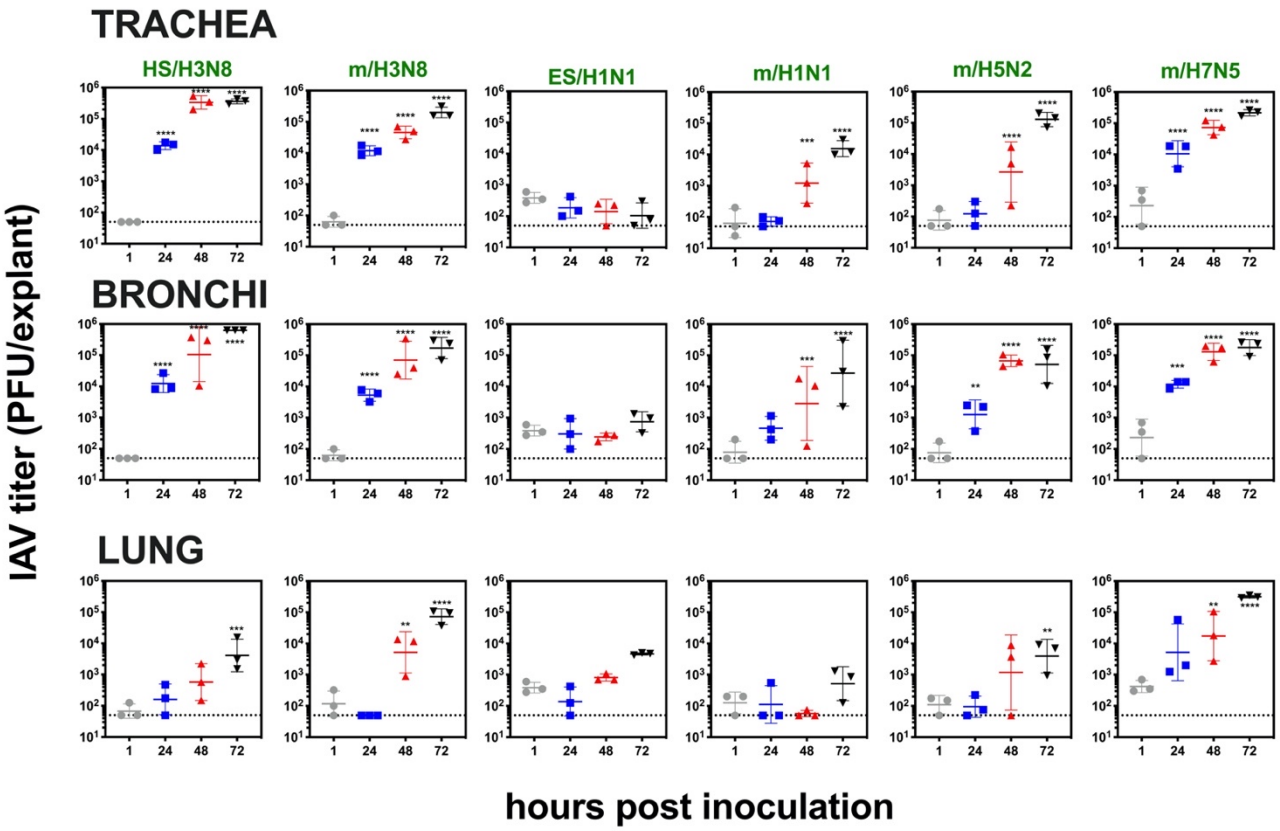

Figure S1. Influenza A virus infection kinetics from 1 to 72 hpi in respiratory tract explants from a 4 year old male rhesus macaque (M15 in Table 2) inoculated with $1X10^4$ PFU of 6 viral strains. Viral titers are represented as the geometric mean and geometric standard deviation. Three explants at each time point were titrated independently and the mean of the triplicates is represented by the middle horizontal line. Asterisks show p values (two-way ANOVA with Dunnett's multiple comparisons) comparing titers at 24, 48 or 72 hpi to 1 hpi, respectively. **p $\leq$ 0.005, ***p < 0.001, and ****p < 0.0001. The dashed line indicates limit of detection, 50 PFU/explant. Strain names refer to the original source of the virus isolate followed by the hemagglutinin and neuraminidase subtype. HS is harbor seal. m is mallard. ES is elephant seal.

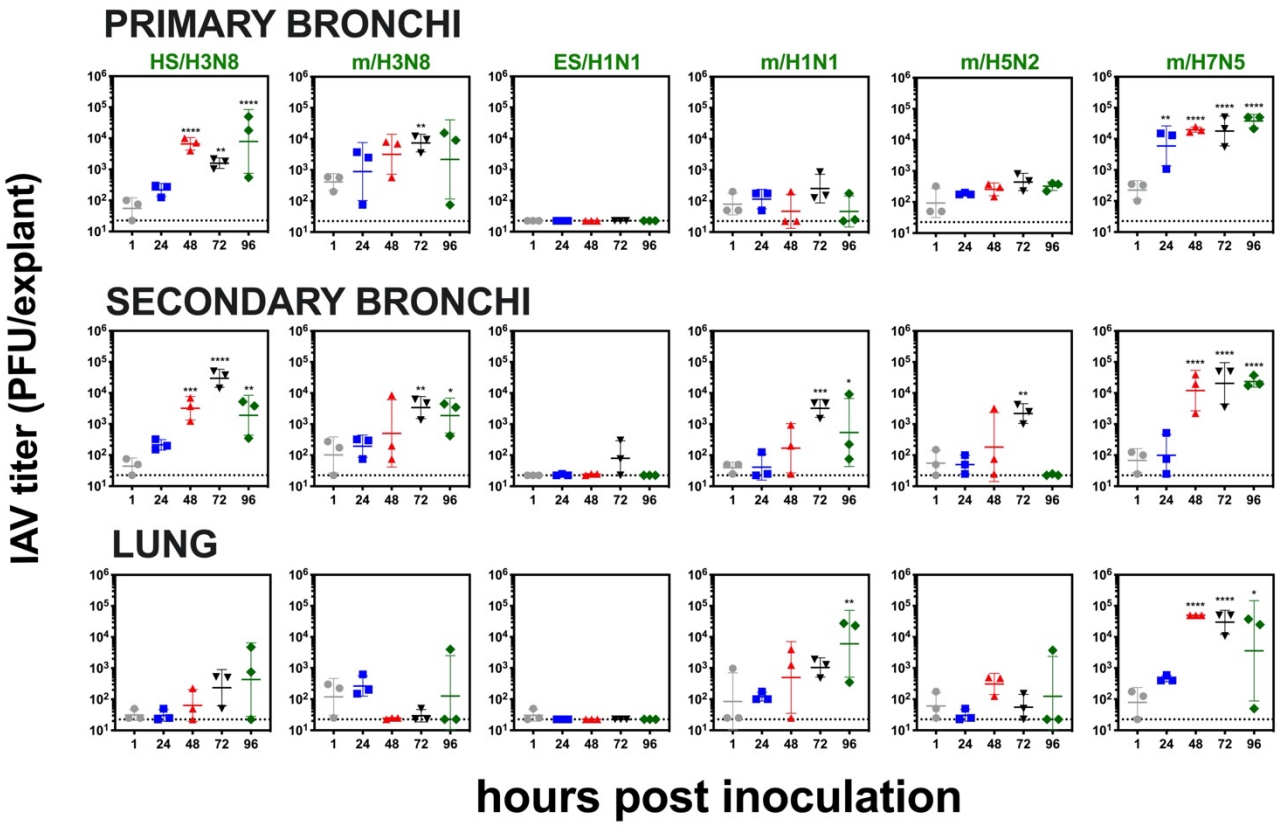

Figure S2. Influenza A virus infection kinetics from 1 to 96 hpi in respiratory tract explants from an adult female California sea lion (SL12 in Table 2) inoculated with $2X10^4$ PFU of 6 IAV strains. Viral titers are represented as the geometric mean and geometric standard deviation. Three explants at each time point were titrated independently and the mean of the triplicates is represented by the middle horizontal line. Asterisks show p values (two-way ANOVA with Dunnett's multiple comparisons) comparing titers at 24, 48, 72 or 96 hpi to 1 hpi, respectively. **p < 0.005, ***p < 0.001, and ****p < 0.0001. The dashed line indicates limit of detection, 50 PFU/explant. Strain names refer to the original source of the virus isolate followed by the hemagglutinin and neuraminidase subtype. HS is harbor seal. m is mallard. ES is elephant seal.

Supplemental Table 1. Mean change in $\log_{10}$ titer of influenza virus strains after inoculation in rhesus macaque or California sea lion respiratory tract explant tissues. Means for the same time frame followed by a common letter are not significantly different by the Games-Howell test at the 5% level of significance. Values in parentheses show standard deviations. The symbols indicate that the mean change in titer differs significantly for at least one strain according to Welch's ANOVA at 5% level of significance for: *1 vs 24 hpi F=15.417, df=(5,91.649), p-value=5.55e-11 for rhesus macaques and F=4.666, df=(5,189.21), p-value=4.85e-04 for California sea lions, the † denotes 1 vs 48 hpi (F=25.823, df=(5,91.569), p-value=3.59e-16) for rhesus macaques and (F=5.784, df=(5,182.59), p-value=5.55e-05) for California sea lions, and the ‡ denotes 72 hpi (F=23.351, df=(5,91.826), p-value=4.58e-15) for rhesus macaques and (F=6.636, df=(5,189.35), p-value=1.02e-05) for California sea lions. Strain names refer to the original source of the virus isolate followed by the hemagglutinin and neuraminidase subtype. HS is harbor seal. m is mallard. ES is elephant seal.

	RHESUS MACAQUES			**CALIFORNIA SEA LIONS**		
	1 vs 24 hpi*	**1 vs 48 hpi†**	**1 vs 72 hpi‡**	**1 vs 24 hpi ***	**1 vs 48 hpi †**	**1 vs 72 hpi ‡**
HS/H3N8	1.2 (1.1) [a]	1.8 (1.5) [ab]	2.2 (1.5) [ad]	0.4 (0.8) [e]	0.6 (1.2) [e]	0.8 (1.4) [e]
m/H3N8	0.9 (1.1) [ac]	1.8 (1.1) [ac]	0.9 (1.4) [ab]	-0.04 (0.7) [abc]	-0.07 (1.1) [abc]	0.2 (1.3) [abc]
ES/H1N1	-0.1 (0.6) [b]	-0.1 (0.8) [e]	0.1 (0.9) [e]	-0.1 (0.5) [ab]	-0.1 (0.8) [ab]	-0.1 (0.9) [ab]
m/H1N1	0.2 (0.7) [b]	0.3 (1.0) [de]	0.9 (1.2) [c]	0.03 (0.6) [bcde]	-0.05 (0.7) [bd]	0.2 (1.0) [bcd]
m/H5N2	0.3 (0.7) [bc]	1.0 (1.4) [bcd]	1.5 (1.4) [bcd]	-0.02 (0.5) [ad]	-0.07 (0.6) [ad]	0.2 (1.0) [ad]
m/H7N5	1.1 (0.8) [a]	1.9 (1.0) [a]	2.4 (1.2) [a]	0.3 (0.9) [cde]	0.5 (1.2) [ce]	0.8 (1.5) [ce]

Supplemental Table 2. Mean change in log_{10} titer of influenza virus in respiratory tract tissues from rhesus macaques and California sea lions. Means for the same time frame followed by a common letter are not significantly different by the Games-Howell test at the 5% level of significance. Values in parentheses show standard deviations. The symbols indicate that the mean change in titer differs significantly for at least one tissue according to Welch's ANOVA at 5% level of significance for: * 1 vs 24 hpi (F=28.071, df=(2, 127.39), p-value=7.93e-11) in rhesus macaques, (F=15.369, df=(2, 269.45), p-value=5.96e-05) for California sea lions, † 1 vs 48 hpi (F=13.641, df=(2, 129.47), p-value=4.02e-6) in rhesus macaques, (F=10.105, df=(2, 257.71), p-value=5.96e-05) in California sea lions, ‡ 1 vs 72 hpi (F=7.8203, df=(2, 133.05), p-value=6.16e-4) for rhesus macaques, (F=11.083, df=(2, 268.89), p-value=2.37e-0.5) for California sea lions.

	RHESUS MACAQUES			**CALIFORNIA SEA LIONS**		
Tissue	**1 vs 24 hpi***	**1 vs 48 hpi†**	**1 vs 72 hpi‡**	**1 vs 24 hpi***	**1 vs 48 hpi†**	**1 vs 72 hpi‡**
Bronchi	1.0 (0.9)[a]	1.5 (1.4) [a]	1.7 (1.5) [a]	0.3 (0.8) [a]	0.5 (1.3) [a]	0.8 (1.5) [a]
Trachea	0.8 (1.0)[a]	1.4 (1.5) [a]	1.9 (1.5) [a]	0.1 (0.7) [a]	0.1 (0.8) [b]	0.2 (1.0) [b]
Lung	0.1 (0.7) [b]	0.5 (1.1) [b]	1.0 (1.4)[b]	-0.2 (0.6) [b]	-0.1 (0.8) [b]	0.1 (1.1) [b]

Supplemental Table 3. **Difference in mean log_{10} change for respiratory tract explant tissues from California sea lions versus rhesus macaques**. Differences are show as p-values after the Games-Howell post-hoc test. Significant *p*-values ($p < 0.05$) are in bold. Strain names refer to the original source of the virus isolate followed by the hemagglutinin and neuraminidase subtype. HS is harbor seal. m is mallard. ES is elephant seal. hpi is hours post inoculation.

Timeframe	IAV Strain	Trachea	Bronchi	Lung
1-24 hpi	HS/H3N8	**-1.26 (0.011)**	**-1.13 (0.023)**	-0.11 (0.989)
	m/H3N8	**-1.26 (0.003)**	**-1.40 (<0.001)**	-0.29 (0.695)
	ES/H1N1	-0.03 (1.00)	-0.13 (0.967)	-0.10 (0.996)
	m/H1N1	-0.14 (0.959)	-0.32 (0.475)	-0.03 (1.00)
	m/H5N2	-0.41 (0.362)	-0.45 (0.388)	-0.07 (0.997)
	m/H7N5	**-1.02 (0.047)**	-0.62 (0.266)	-0.46 (0.551)
1-48 hpi	HS/H3N8	**-1.95 (0.002)**	-1.27 (0.120)	-0.18 (0.982)
	m/H3N8	**-2.21 (<0.001)**	**-1.50 (0.009)**	**-1.50 (0.006)**
	ES/H1N1	-0.02 (1.00)	0.25 (0.963)	-0.45 (0.572)
	m/H1N1	-0.74 (0.160)	-0.48 (0.714)	0.01 (1.00)
	m/H5N2	-0.99 (0.100)	**-1.50 (0.024)**	-0.25 (0.918)
	m/H7N5	**-1.75 (<0.001)**	**-1.50 (0.001)**	-0.71 (0.540)
1-72 hpi	HS/H3N8	**-2.41 (<0.001)**	**-1.74 (0.015)**	-0.49 (0.711)
	m/H3N8	**-2.02 (<0.001)**	-1.44 (0.085)	**-1.87 (0.006)**
	ES/H1N1	-0.05 (1.00)	0.01 (1.00)	-0.48 (0.464)
	m/H1N1	-0.83 (0.265)	-1.06 (0.131)	-0.03 (1.00)
	m/H5N2	**-2.11 (<0.001)**	-1.23 (0.083)	-0.32 (0.893)
	m/H7N5	**-2.16 (<0.001)**	-1.08 (0.229)	-1.11 (0.335)

Supplemental Table 4. **Immunohistochemical detection of influenza A virus in macaque and California sea lion respiratory tissue explants.** Strain names refer to the original source of the virus isolate followed by the hemagglutinin and neuraminidase subtype. HS is harbor seal. m is mallard. ES is elephant seal. hpi is hours post inoculation.

	IAV positive epithelial cells/mm^2							
Animal	**M11**		**M13**		**SL08**		**SL12**	
hpi	**24**	**48**	**24**	**48**	**24**	**48**	**24**	**48**
HS/H3N8	458	519	71	224	0	0	51	21
m/H3N8	349	544	0	1	2	0	0	26
ES/H1N1	0	0	0	0	0	0	0	0
m/H1N1	0	8	0	0	0	0	0	0
m/H5N2	7	19	0	0	0	0	0	0
m/H7N5	50	626	9	0	0	0	8	<5

Supplemental Table 5. **IAV inoculated rhesus macaque and marine mammal respiratory tract explants from which whole genome IAV sequences were obtained at indicated times post-inoculation and compared to their respective inocula**. Empty squares indicate samples for which sequencing was not attempted. HS is harbor seal. m is mallard. ES is elephant seal, M is macaque, SL is California sea lion.

		hour(s) post inoculation					
Animal ID	**tissue**	**HS/H3N8**	**m/H3N8**	**ES/H1N1**	**m/H1N1**	**m/H5N2**	**m/H7N5**
M15	trachea	72	72		72	72	72
	lung						72
M11	trachea	72	72		72		72
SL01	bronchi		72				72, 96
SL06	bronchi	48, 72	72			72	48, 72
SL08	trachea						48
	bronchi			72			72
ES10	bronchi	48, 72					

Supplemental Table 6. **IAV amino acid changes compared to inocula detected in *ex vivo* bronchi explants from California sea lions and a Northern elephant seal**. Numbers shown correspond to positions in indicated IAV proteins. *Indicates that the mutation was a synonymous change. Empty squares indicate no sequence differences were detected. An X shows samples for which sequencing was not attempted. hpi is hours post inoculation, HS is harbor seal, m is mallard, ES is elephant seal, M is macaque, SL is California sea lion, HA is hemagglutinin, NA is neuraminidase, PA is polymerase acidic protein, PB is polymerase basic protein.

Animal ID	hpi	HS/H3N8 HA	HS/H3N8 NA	ES/H1N1 PA	m/H7N5 HA	m/H7N5 PB2*
SL01	72	X	X	X	V311I	1368
	96		V394I	X		
SL06	48			X		1368
	72		P118S	X		1368
SL08	48	X	X	X		1368
	72	X	X	I359N M441I		1368
ES10	48	A154T	P118S	X	X	X
	72	A154T	P118S	X	X	X

REFERENCES FOR SUPPLEMENT

1. T. Goldstein, *et al.*, Pandemic H1N1 Influenza Isolated from Free-Ranging Northern Elephant Seals in 2010 off the Central California Coast. *PLoS One* (2013) https:/doi.org/10.1371/journal.pone.0062259.

2. E. A. Karlsson, *et al.*, Respiratory transmission of an avian H3N8 influenza virus isolated from a harbour seal. *Nat. Commun.* (2014) https:/doi.org/10.1038/ncomms5791.

3. X. Deng, *et al.*, Genomic surveillance reveals multiple introductions of SARS-CoV-2 into Northern California. *Science* (2020) https:/doi.org/10.1126/science.abb9263.

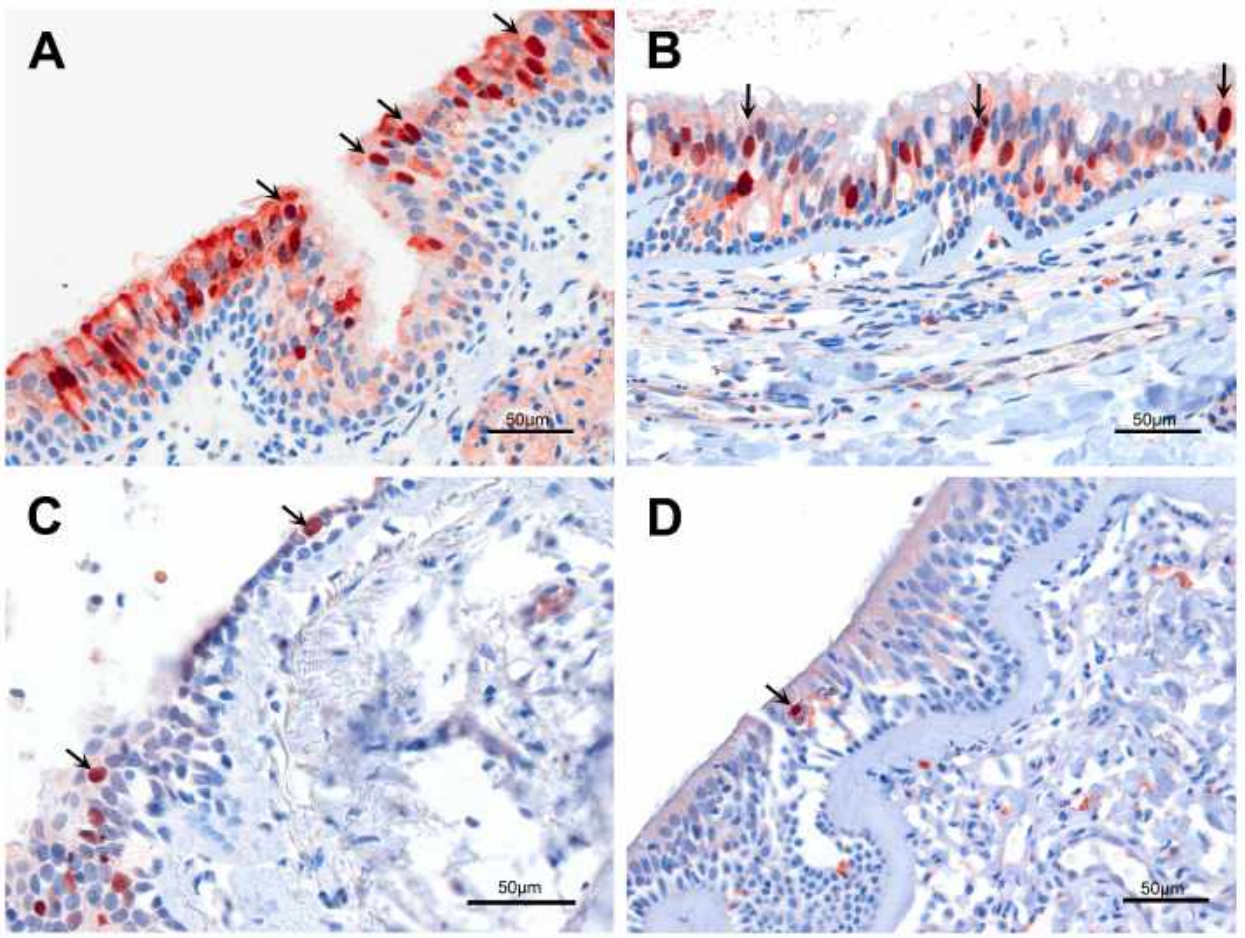

Figure 5. Photomicrographs of positive immunohistochemical (IHC) staining against influenza A virus in rhesus macaque and California sea lion tracheal and bronchial explants. (A) Trachea from rhesus macaque M11 48 hours post inoculation with m/H7N5; **(B)** Trachea from rhesus macaque M13, 48 hours post-inoculation with HS/H3N8; **(C)** Bronchus from sea lion SL12 48 hours post inoculation with av/H3N8; **(D)** Trachea from California sea lion SL08 24 hours post inoculation with av/H3N8. Positive respiratory epithelial cells exhibit strong nuclear immunoreactivity (red-brown nuclear staining; arrows). Positive staining is primarily localized to apical epithelial cells, with relative sparing of basal cells. IHC stain used an antibody against influenza A virus nucleoprotein. Bar=50um.